

This is the Post-print version of the following article: *Gerardo Daniel-Pérez, J.L. Sánchez Llamazares, P. Alvarez-Alonso, C.F. Sánchez-Valdés, R. Varga, V. Chernenko, A. Quintana-Nedelcos, Transformation behavior and magnetocaloric effect in Mn_{1-x}Cr_xCoGe (x=0.04 and 0.11) melt-spun ribbons tailored by heat treatment, Journal of Magnetism and Magnetic Materials, Volume 444, 2017, Pages 263-269*, which has been published in final form at: <https://doi.org/10.1016/j.jmmm.2017.08.016>

© 2017. This manuscript version is made available under the CC-BY-NC-ND 4.0 license <http://creativecommons.org/licenses/by-nc-nd/4.0/>

Accepted Manuscript

Transformation behavior and magnetocaloric effect in $\text{Mn}_{1-x}\text{Cr}_x\text{CoGe}$ ($x = 0.04$ and 0.11) melt-spun ribbons tailored by heat treatment

Gerardo Daniel-Pérez, J.L. Sánchez Llamazares, P. Alvarez-Alonso, C.F. Sánchez-Valdés, R. Varga, V. Chernenko, A. Quintana-Nedelcos

PII: S0304-8853(17)30987-3

DOI: <http://dx.doi.org/10.1016/j.jmmm.2017.08.016>

Reference: MAGMA 63050

To appear in: *Journal of Magnetism and Magnetic Materials*

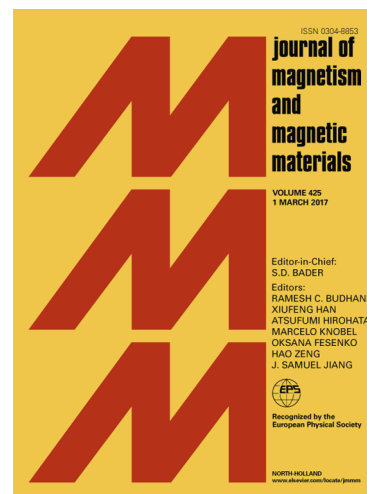
Received Date: 26 March 2017

Revised Date: 7 July 2017

Accepted Date: 4 August 2017

Please cite this article as: G. Daniel-Pérez, J.L. Sánchez Llamazares, P. Alvarez-Alonso, C.F. Sánchez-Valdés, R. Varga, V. Chernenko, A. Quintana-Nedelcos, Transformation behavior and magnetocaloric effect in $\text{Mn}_{1-x}\text{Cr}_x\text{CoGe}$ ($x = 0.04$ and 0.11) melt-spun ribbons tailored by heat treatment, *Journal of Magnetism and Magnetic Materials* (2017), doi: <http://dx.doi.org/10.1016/j.jmmm.2017.08.016>

This is a PDF file of an unedited manuscript that has been accepted for publication. As a service to our customers we are providing this early version of the manuscript. The manuscript will undergo copyediting, typesetting, and review of the resulting proof before it is published in its final form. Please note that during the production process errors may be discovered which could affect the content, and all legal disclaimers that apply to the journal pertain.



Transformation behavior and magnetocaloric effect in $\text{Mn}_{1-x}\text{Cr}_x\text{CoGe}$ ($x = 0.04$ and 0.11) melt-spun ribbons tailored by heat treatment

Gerardo Daniel-Pérez^a, J.L. Sánchez Llamazares^{b,*}, P. Alvarez-Alonso^c, C.F. Sánchez-Valdés^d, R. Varga^e, V. Chernenko^{f,g}, A. Quintana-Nedelcos^h

^a Instituto Tecnológico Superior de Irapuato, 36821 Irapuato, Guanajuato, México

^b División de Materiales Avanzados, Instituto Potosino de Investigación Científica y Tecnológica A.C., Camino a la presa San José 2055, 78216 San Luis Potosí, SLP, México

^c Departamento de Física, Universidad de Oviedo, 33007 Oviedo, Spain

^d División Multidisciplinaria, 32579 Ciudad Universitaria, Universidad Autónoma de Ciudad Juárez (UACJ), calle José de Jesús Macías Delgado # 18100, Ciudad Juárez, Chihuahua, México

^e Institute of Physics, Faculty of Sciences, University Pavol Jozef Safárik, Park Angelinum 9, 04154, Kosice, Slovakia.

^f BCMaterials and University of Basque Country, UPV/EHU, Bilbao, 48080, Spain

^g Ikerbasque, Basque Foundation for Science, 48013 Bilbao, Spain

^h Department of Materials Science and Engineering, University of Sheffield, Sheffield S1 3JD, United Kingdom

ABSTRACT

Recently, MnNiGe and MnCoGe intermetallic compounds have received a considerable attention due to the coupled tunable martensitic and magnetic transitions as well as giant magnetocaloric effect (MCE) they exhibit. In this work, by doping with Cr and varying of the annealing regime, a merged magnetostructural transition between a ferromagnetic orthorhombic and a paramagnetic hexagonal structure was received near room temperature in $\text{Mn}_{1-x}\text{Cr}_x\text{CoGe}$ melt-spun ribbons with $x = 0.04$ and 0.11 . Structural and magnetic characterizations have been performed by X-ray diffraction, differential scanning calorimetry and magnetization measurements. It is found that, in ribbons with $x = 0.04$ (0.11) annealed at 1148 K, the peak value of the magnetic entropy change and the refrigerant capacity through the orthorhombic to hexagonal transition strongly increase with the annealing time from 7.3 (9.4) $\text{Jkg}^{-1}\text{K}^{-1}$ to 10.6 (13.7) $\text{Jkg}^{-1}\text{K}^{-1}$ and from 182 (235) Jkg^{-1} to 214 (267) Jkg^{-1} , respectively, at 5 T for the time increase from 4 h to 8 h. Compared to bulk alloys of similar composition, the fabricated melt-spun ribbons show much broader working temperature range and a higher cooling efficiency.

Keywords: MnCrCoGe melt-spun ribbons; martensitic transformation; magnetostructural transition; magnetocaloric effect.

* Corresponding author. Email address: jose.sanchez@ipicyt.edu.mx (J.L. Sánchez Llamazares).

1. Introduction

Currently, ferromagnetic (FM) alloys presenting a tunable first-order martensitic transformation (MT) near room temperature accompanied by a large and steep magnetization change, ΔM , are intensively investigated due to their potential as candidates for magnetic refrigeration technology in this temperature range [1,2]. Among them, MnCoGe-based alloys represent an interesting family of magnetocaloric (MC) materials owing to the possibility to merge the martensitic and the magnetic phase transitions, usually giving rise to giant MC effects [1,3].

In the stoichiometric MnCoGe alloy, the structural transformation between the hexagonal and orthorhombic phases occurs at $T > 398$ K [4,5]; around such temperatures, both phases are paramagnetic (PM) as their respective Curie temperatures are reported to be $T_C^{\text{hex}} = 275$ K and $T_C^{\text{orth}} = 355$ K [6,7]. After a prolonged thermal annealing of a bulk sample at an appropriate temperature, the structural transformation temperature T_{str} can be tuned within the temperature window delimited by both T_C^{hex} and T_C^{orth} , i.e., $T_C^{\text{hex}} < T_{\text{str}} < T_C^{\text{orth}}$, resulting in a coupled magnetostructural transformation upon cooling from a high-temperature PM hexagonal Ni₂In-type phase (space group P6₃/mmc; referred to as austenite phase) to a low-temperature FM orthorhombic phase with a TiNiSi-type structure (space group Pnma; referred to as martensite phase). Thus, the ΔM associated to this coupled magnetic and structural transition frequently leads to large peak isothermal magnetic entropy change $|\Delta S_M^{\text{peak}}|$ [1,8].

Recently, effective ways of pushing T_{str} inside the $T_C^{\text{hex}} - T_C^{\text{orth}}$ temperature range whereby achieving the magnetostructural transition have been suggested: (i) by stoichiometry changes [9]; (ii) by replacing a small amount of one of the three basic constituents by a fourth one, such as Cr [10,11], V [12], Ti [13], Ga [14], and/or; (iii) by adding a small amount of a fourth element as B [3,8], or C [15]. The effect of Mn substitution for Cr on the martensitic phase transition temperature and MC properties of the bulk MnCoGe alloys was first reported by Trung *et al.* [10,15]. In the series Mn_{1-x}Cr_xCoGe with $x = 0.04, 0.11, 0.18, 0.25$ and 0.27 , thermally annealed at 1123 K for 5 days, they found that the magnetostructural transition temperature decreases upon increasing of the Cr content; samples with $x = 0.04$ and 0.11 showed the largest giant magnetic entropy change peak values $|\Delta S_M^{\text{peak}}|$ around room temperature ($|\Delta S_M^{\text{peak}}| \sim 28 \text{ Jkg}^{-1}\text{K}^{-1}$ under a magnetic field change $\mu_0\Delta H$ from 0 to 5 T).

Rapid solidification by the melt-spinning technique has been used to obtain single phase MnCoGe-based ribbons with enhanced MC properties [7,8]. Besides, for any practical application melt-spun ribbons are precursors that can be consolidated by sintering techniques to achieve a desired geometry [16]. Previously, we have reported on the MC properties of MnCoGe [7], and MnCoGeB_{0.01} [8] melt-spun ribbons related to the ferromagnetic second order transition in the Ni₂In-type and TiNiSi-type

crystal structures, and their coupled first-order magnetostructural transition, respectively. In this contribution, we report the synthesis and the effect of thermal annealing temperature and time on the magnetostructural transition temperature and magnetic entropy change in the $\text{Mn}_{1-x}\text{Cr}_x\text{CoGe}$ ($x = 0.04$ and 0.11) melt spun ribbons. The results are compared with those reported in literature for bulk alloys [10].

2. Experimental procedure

$\text{Mn}_{1-x}\text{Cr}_x\text{CoGe}$ ribbons with $x = 0.04$ and 0.11 at. %, were fabricated by melt-spinning in Ar atmosphere from arc-melted ingots previously produced from high purity elements (Co 99.99%, Mn 99.99%, Cr 99.98%, and Ge 99.99%). An injection pressure of 0.3 bar was employed to eject the molten alloy onto the polished surface of copper wheel rotating at a linear speed of 20 ms^{-1} . The process was carried out in an Edmund Buehler model SC melt spinner system. As-solidified ribbons were sealed in quartz ampoules under Ar (0.5 bar), annealed at temperatures between 923 K and 1148 K during 4 or 8 hours and quenched in water.

The starting and finishing direct and reverse martensitic transformation temperatures, i.e., M_S , M_f , A_S and A_f , were determined by the standard tangential method from the differential scanning calorimetric (DSC) curves measured with a TA-Instruments Q200 DSC system. Room temperature X-ray diffraction (XRD) patterns were collected by a Bruker AXS D8 Advance diffractometer with $\text{CuK}\alpha$ radiation, and analyzed using Rietveld refinement implemented in the FullProf suite [17]. The reliability of the Rietveld fits for the thermally annealed samples studied is expressed by the R_{exp} , and χ^2 in Table 1. The microstructural study presented below (see Fig. 6) was carried out using a Hitachi TM 3000 Tabletop scanning electron microscope (SEM) equipped with a Peltier cooling system.

Magnetization as a function of temperature curves, $M(T)$, were measured in the temperature range of 200 K - 400 K, with a heating/cooling rate of 1.0 Kmin^{-1} , under constant applied magnetic fields of 5 mT and 5 T using the vibrating sample magnetometer module of a Quantum Design Evercool-I PPMS system. The magnetic field $\mu_0 H$ was applied along the ribbon length to minimize the demagnetizing field effect. The MC effect was studied by determining the temperature dependence of the magnetic field induced entropy change, $\Delta S_M(T)$, through numerical integration of the Maxwell relation from a set of magnetization isotherms, $M(\mu_0 H)$. The thermal protocol followed to measure each magnetization isotherm through the orthorhombic to hexagonal phase transition was as follows: at zero magnetic field the sample was heated to 400 K to stabilize hexagonal phase, cooled to 200 K to form orthorhombic

one, and then heated again in no-overshot mode to the selected measuring temperature T_{meas} . As discussed in reference 8, this thermal cycling ensures that prior to apply the magnetic field at a given T_{meas} the sample shows the phase constitution that correspond to the thermally induced structural transition.

Refrigerant capacity (RC) was estimated making use of the following three different criteria: $RC-1 = |\Delta S_M^{\text{peak}}| \times \delta T_{\text{FWHM}}$, $RC-2 = \int_{T_{\text{cold}}}^{T_{\text{hot}}} [\Delta S_M(T)]_{\mu_{oH}} dT$, and $RC-3$ according to the Wood and Potter method [18]. This physical quantity characterizes the effective amount of heat that might be transferred from the hot to the cold sink if an ideal refrigeration cycle is considered. In case of $RC-1$ and $RC-2$, δT_{FWHM} is the temperature interval corresponding to the full-width at half-maximum of the $\Delta S_M(T)$ curve that is delimited by the temperatures T_{hot} and T_{cold} . $\delta T_{\text{FWHM}} = T_{\text{hot}} - T_{\text{cold}}$ is usually assumed as the useful working temperature range of a MC refrigerant.

3. Results and discussion

Fig. 1 depicts the temperature dependences of the magnetization measured at 5 mT for as-solidified $\text{Mn}_{1-x}\text{Cr}_x\text{CoGe}$ melt-spun ribbons with $x = 0.04$ and 0.11 . They show in each ribbon the existence of single ferromagnetic phase with the Curie temperature T_C^{hex} of 225 K and 255 K, respectively. To date no other results have been reported in literature for bulk alloys to compare these data. The corresponding room temperature X-ray powder diffraction patterns (shown at the inset of Fig. 1), reveal the formation of the hexagonal Ni_2In -type phase with the following lattice constants: $a = 4.083(1) \text{ \AA}$, and $c = 5.307(1) \text{ \AA}$ for $x = 0.04$, and $a = 4.085(1) \text{ \AA}$, and $c = 5.306(1) \text{ \AA}$ for $x = 0.11$. It is worth noting that the XRD patterns do not allow distinguishing any preferential orientation; moreover, the formation of a single-phase hexagonal phase is consistent with the previously observed in stoichiometric MnCoGe [7], $\text{MnCoGeB}_{0.01}$ [8], and $\text{Mn}_{0.96}\text{Co}_{1.04}\text{GeB}_{0.02}$ [19] melt-spun ribbons. DSC curves for the as-solidified ribbons, depicted in Fig. 2(a) and Fig. 3(a), do not show any structural transition further confirming that the hexagonal single-phase with the Ni_2In -type structure formed from the melt in as-solidified ribbons is stable.

Annealing at the temperature 923 K/4h leads to the appearance of the structural transition (see the DSC curves in Figs. 2(a) and 3(a)) with characteristic temperatures above room temperature. The thermal hysteresis of the transformation ΔT_{hys} , was estimated as $\Delta T_{\text{hys}} = A_f - M_S$. The values of these characteristic temperatures for the thermally annealed samples are given in Table 1. It must be noted that samples show wide transition ranges of 56 K (36 K) and 34 K (25 K) for direct and reverse transformations for $x = 0.04$ (0.11), respectively (see also Table 1). Note also that ΔT_{hys} is large and

similar for both samples (30 and 35 K for $x = 0.04$ and 0.11 , respectively), resulting around 3 times larger than the found (~ 10 - 12 K) for the bulk samples of similar composition as reported in [10,15]. The room temperature X-ray powder diffraction patterns for these two samples are depicted in Fig. 4(a) and Fig. 5(a), and point to the coexistence of two phases: the high-temperature one with the hexagonal crystal structure (lattice constants $a = 4.089(3)$ Å and $c = 5.306(5)$ Å) and the low-temperature one with the orthorhombic crystal structure ($a = 5.967(4)$ Å, $b = 3.816(3)$ Å and $c = 7.043(5)$ Å) for $x = 0.04$ and hexagonal ($a = 4.084(2)$ Å and $c = 5.310(2)$ Å) and orthorhombic (with $a = 5.951(1)$ Å, $b = 3.818(1)$ Å and $c = 7.042(3)$ Å) in sample with $x = 0.11$. The volume fraction of the hexagonal (orthorhombic) phase obtained from the Rietveld analysis was 13 ± 2 % (87 ± 2 %) for $x = 0.04$ and 14 ± 2 % (86 ± 2 %) for $x = 0.11$. Notice that, as previously observed [7,19,20], a volume fraction of the hexagonal phase always coexists with the orthorhombic one.

Increasing of the annealing temperature to 1123 K, and to 1148 K, while keeping 4 hours of annealing time: (a) the structural phase transition temperature decreases approaching to room temperature; (b) the thermal hysteresis of the structural transition for $\text{Mn}_{0.96}\text{Cr}_{0.04}\text{CoGe}$ ribbons remains around the same value (~ 30 K), while for $\text{Mn}_{0.89}\text{Cr}_{0.11}\text{CoGe}$ ribbons reduces around ~ 10 - 12 K. By doubling the annealing time at 1148 K, from 4 to 8 hours, no significant impact on ΔT_{hys} was observed (see Table 1). The large thermal hysteresis is an important drawback of these alloys as first-order magnetic refrigerants. In line with the cooling DSC paths, the room-temperature XRD patterns of samples annealed at 1123 K and 1148 K (see Figs. 4 and 5) reveal that the major phase is the hexagonal one.

It is known that MnCoGe-based alloys undergoing MT show the so-called “virgin effect” [8,15], a phenomenon that has been also observed in other Mn-based alloys such as MnFe(P,X) ($X = \text{As}, \text{Si}, \text{Ge}$) [21,22] and MnAs-based compounds [15]. This is, in the first MT after synthesis (i.e., on the first cooling), the cooling DSC curve discloses that the hexagonal to orthorhombic phase transition appears at a well lower temperature than that found in the second and any subsequent cooling cycle. On the contrary, the transition on heating always occurs with approximately the same starting and finishing transition temperatures. This effect for the studied alloy ribbons is illustrated in the top graph of Fig. 6 for the sample with $x = 0.11$ annealed at 923 K during 4h. The sequence of SEM images shown at the bottom of Fig. 6 illustrates the progressive cracking process experienced by a virgin sample during its first cooling process. This results from the high cell volume change between the hexagonal and the orthorhombic phase through the transition (~ 4 %) [4]. The mechanical deterioration of these alloys is a serious disadvantage from the point of view of any practical application.

Fig. 7 serves to illustrate the coupled magnetostructural transition occurring between the orthorhombic and the hexagonal phase; the data correspond to the ribbon samples with $x = 0.04$ annealed at 1148 K during 4 hours. Whereas Fig. 7(a) shows the heating/cooling $M(T)$ and DSC curves, the room temperature X-ray diffraction patterns, plotted in Figs. 7(b) and (c), denote the sample phase constitution in points A and B, respectively. Point A corresponds to a temperature slightly above M_s , thus the sample is paramagnetic and hexagonal; decreasing the temperature, the sample transforms into the orthorhombic ferromagnetic phase, while the small shoulder around 225 K reveals the presence of small amount of hexagonal phase (corroborated by the XRD pattern in point B) coexisting with the orthorhombic one.

Figures 8(a) and (b) show the typical shape of the isothermal magnetization $M(\mu_0 H)$ curves measured for the annealed samples that show a coupled magnetostructural transition from a major ferromagnetic orthorhombic phase to a paramagnetic hexagonal one increasing the applied magnetic field up to 5 T; for the figure, we selected ribbon samples with $x = 0.04$ and 0.11 annealed at 1148 K during 8 hours. Notice that the curves do not evidence the occurrence of field-induced metamagnetic transition. Figures 8(c) and (d) display the isothermal magnetization curves measured on increasing the magnetic field up to 2 T (field-up) and removing the field to zero (field-down). As shown, the $M(\mu_0 H)$ curves are fully reversible because on heating the structural transition is only of thermal nature (i.e., the magnetic field does not transform a fraction of the orthorhombic phase into the hexagonal one); therefore, across the structural phase transition on heating no hysteresis losses appear. In these materials, the transition that can be promoted by the effect of the magnetic field is in the opposite direction, as has been experimentally demonstrated [8,12,23].

Figures 9(a) and (b) show the thermal dependence of the magnetic entropy change for the annealed samples of both compositions for magnetic field changes of 2 and 5 T; significant MC properties derived from the curves, such as $|\Delta S_M^{\text{peak}}|$, δT_{FWHM} , and RC , are listed in Table 2 (as isothermal magnetization curve are reversible, RC values are net values). The inserted graphs in the figure display the heating/cooling $M(T)$ curves recorded under a field of 5 T; the drawn arrows serve to indicate their heating and cooling branches. In these alloys, the magnetic field-induced entropy change peaks at the temperature that corresponds to the magnetostructural transition, except when the structural transition is above T_C^{orth} that the magnetization decrease is due to the second-order transition of the orthorhombic phase. It must be noticed that the temperature of the peak does not change with $\mu_0 \Delta H$; also, δT_{FWHM} is almost constant. To the measured magnetic field induced entropy change in samples with magnetostructural transition contributes the lattice and magnetic structure changes. The measured

$|\Delta S_M^{\text{peak}}|$ values for samples annealed at 1123 K and 1148 K are large but lower than those reported for bulk samples of similar composition for the same magnetic field change [10,15]. The transformation temperature of the ribbons are close but differs from the one found in bulk samples. But, as previously shown for $\text{Mn}_{0.96}\text{Co}_{1.04}\text{GeB}_{0.02}$ alloy ribbons [19], keeping the annealing time the characteristic structural transition temperature for the first-order transition may strongly decrease, 110-120 K about, with the increase of the annealing temperature. Notice that, even when no systematic study was carried out on this issue, in the present ribbons the increase in the annealing time from 4 to 8 hours also shifts the transition temperature. $|\Delta S_M^{\text{peak}}|$ tends to increase with the increasing of annealing temperatures and annealing times reaching the highest values in samples annealed at 1148 K for 8 h (10.6 and 13.7 $\text{Jkg}^{-1}\text{K}^{-1}$ for $x = 0.04$ and 0.11, respectively). A $|\Delta S_M^{\text{peak}}|$ value equal to 13.1 $\text{Jkg}^{-1}\text{K}^{-1}$ ($\mu_0\Delta H = 2$ T) has been reported for melt-spun ribbons of nominal composition $\text{Mn}_{0.98}\text{Cr}_{0.02}\text{CoGe}$ annealed at 1073 K for one hour [24]. The lower $|\Delta S_M^{\text{peak}}|$ values shown by our samples, compared with others of close composition, can be ascribed to the broader temperature interval of the magnetostructural transformation (see, for instance, Fig. 7). On the other hand, this fact yields an advantage for our materials since the refrigerant capacity (RC) is enhanced due to the widening of the working temperature range (δT_{FWHM}). As the RC parameter is proportional to the area below the $\Delta S_M(T)$ curve, our samples show similar or superior values than those obtained in bulk materials of similar composition annealed at 1123 h for the extremely long time of 120 h [10], but the operating temperature range is around three times larger. The $\text{Mn}_{0.96}\text{Cr}_{0.04}\text{CoGe}$ ribbons and bulk show similar values of $RC-1$, of about 90 Jkg^{-1} for $\mu_0\Delta H = 2$ T and about 235 Jkg^{-1} for $\mu_0\Delta H = 5$ T. In the $\text{Mn}_{0.89}\text{Cr}_{0.11}\text{CoGe}$ ribbons, $RC-1$ value is larger by 25 Jkg^{-1} ($\mu_0\Delta H = 2$ T) and by 64 Jkg^{-1} ($\mu_0\Delta H = 5$ T) than the RC value found in bulk materials.

4. Conclusions

The effect of thermal annealing on the magnetostructural transition temperatures and magnetocaloric properties of melt-spun $\text{Mn}_{1-x}\text{Cr}_x\text{CoGe}$ ribbons with $x = 0.04$ and 0.11, was studied. We observed that as-solidified samples crystallize into a single hexagonal phase with the Ni_2In -type crystal structure, which is stable during subsequent cooling below room temperature and exhibiting ferromagnetic ordering at $T_C^{\text{hex}} = 225$ K (for $x = 0.04$ ribbon) and 255 K (for $x = 0.11$ ribbon). The reduced values of T_C^{hex} in comparison to $T_C^{\text{hex}} = 275$ K of the melt-spun [7] and bulk ternary MnCoGe alloys [3,6] is attributed to the influence of Cr doping. Annealing times needed to produce the martensitic transformation from the hexagonal to the orthorhombic phase was considerably reduced from typically

few days in bulk samples to few hours in melt-spun ribbons: a similar transformation behavior in the ribbons and bulk samples has been obtained after annealing time of 4 - 8 hours at 1148 K in the former sample and 120 hours at 1123 K in the latter ones. The mechanical deterioration of these alloys owing to the multiple cracks that appear during the structural transition process, as well as the large thermal hysteresis of the structural transformation, are serious drawbacks from the application point of view. The best performance in terms of $|\Delta S_M^{\text{peak}}|$ and RC values was found in ribbons annealed at 1148 K for 8 hours. Yet, they show the lower values of $|\Delta S_M^{\text{peak}}|$ than the reported for bulk alloys of similar composition, it is important to highlight that they show a similar or even higher refrigerant capacity (at $\mu_0\Delta H = 5$ T, $RC-1$ values for $x = 0.04$ annealed at 1148 K during 4 and 8 h are 182 and 235 Jkg^{-1} ; whereas for $x = 0.11$ annealed at 1148 K with the same annealing time are 214 and 267 Jkg^{-1}) in a much broader working temperature range ($\delta T_{\text{FWHM}} = 20-24$ K) than the bulk samples (at $\mu_0\Delta H = 5$ T, $RC-1 = 228$ Jkg^{-1} and 203 Jkg^{-1} for $\text{Mn}_{0.96}\text{Cr}_{0.04}\text{CoGe}$ and $\text{Mn}_{0.89}\text{Cr}_{0.11}\text{CoGe}$, respectively).

Acknowledgements. This work was financially supported by grants CB-2012-01-183770 (CONACYT, Mexico), Asturias Government, Spain (FC-15-GRUPIN14-037 245), and MAT2014-56116-C4-3-4-R (MINECO, Spain). This work was technically supported by LINAN (IPICYT) where most of the experiments were carried out. The technical support of Dr. G.J. Labrada-Delgado, and M.Sc. B.A. Rivera-Escoto is gratefully acknowledged. C.F. Sánchez-Valdés is grateful to DMCU-UACJ for supporting his research stay at IPICYT (program PFCE and academic mobility grant); the financial support received from CONACYT and PRODEP-SEP, Mexico, is also acknowledged.

References

- [1] K.A. Gschneidner, Y. Mudryk, V.K. Pecharsky, *Scr. Mater.* 67 (2012) 572.
- [2] S. Crossley, N.D. Mathur, X. Moya, *AIP Adv.* 5 (2015) 67153.
- [3] N.T. Trung, L. Zhang, L. Caron, K.H.J. Buschow, E. Brück *Appl. Phys. Lett.* 96 (2010) 172504.
- [4] V. Johnson, *Inorg. Chem.* vol. 14 (5) (1975) 117–120.
- [5] S. Niziol, A. Weselucha, B. Bazela, A. Szytula, *Solid State Commun.* 39 (1981) 1081.
- [6] A. Szytula, A. T. Pedziwiatr, Z. Tomkowicz, *J. Magn. Magn. Mater.* 25 (1981) 176.
- [7] C.F. Sánchez-Valdés, J.L. Sánchez Llamazares, H. Flores-Zúñiga, D. Ríos-Jara, P. Alvarez-Alonso, P. Gorria, *Scr. Mater.* 69 (2013) 211.
- [8] A. Quintana-Nedelcos, J.L. Sánchez Llamazares, C.F. Sánchez-Valdés, P. Álvarez Alonso, P. Gorria, P. Shamba, N. A. Morley, *J. Alloys Compd.* 694 (2017) 1189.
- [9] J.T. Wang, D. S. Wang, C. Chen, O. Nashima, T. Kanomata, H. Mizuseki, Y. Kawazoe, *Appl. Phys. Lett.*, 89 (2006) 262504.
- [10] N.T. Trung, V. Biharie, L. Zhang, L. Caron, K.H.J. Buschow, E. Brück, *Appl. Phys. Lett.* 96 (2010) 162507.
- [11] J. Torrens-Serra, C.A. Biffi, R. Santamarta, V. Recarte, J.I. Pérez-Landazábal, A. Tuissi, E. Cesari, *Mater. Charact.* 93 (2014) 24.
- [12] S.C. Ma, Y.X. Zheng, H.C. Xuan, L.J. Shen, Q.Q. Cao, D.H. Wang, Z.C. Zhong, Y.W. Du, *J. Magn. Magn. Mater.* 324 (2012) 135.
- [13] P. Shamba, J.L. Wang, J.C. Debnath, S.J. Kennedy, R. Zeng, M.F.M. Din, F. Hong, Z.X. Cheng, A.J. Studer, S.X. Dou, *J. Physics. Condens. Matter* 25 (2013) 56001.
- [14] E. Yüziak, G. Durak, I. Dincer, Y. Elerman, *J. Alloys Compd.* 541 (2012) 256.
- [15] N.T. Trung, *First-order phase transitions and giant magnetocaloric effect*, Ph.D. thesis Technische Universiteit Delft, 2010 (ISBN/EAN: 978-90-8593-081-5).
- [16] V.V Khovaylo, V.V Rodionova, S.N. Shevyrtalov, V. Novosad, *Phys. Status Solidi* 251 (2014) 2104.
- [17] J. Rodríguez-Carvajal, *Physica B Condens. Matter* 192 (1992) 55.
- [18] M.E. Wood, W.H. Potter, *Cryogenics* 25 (1985) 667.
- [19] A. Quintana-Nedelcos, J.L. Sánchez Llamazares, H. Flores-Zúñiga, *J. Alloys Compd.* 644 (2015) 1003.
- [20] G. Daniel-Perez, J.L. Sanchez Llamazares, A. Quintana-Nedelcos, P. Alvarez-Alonso, R. Varga, V. Chernenko, *J. Appl. Phys.* 115 (2014) 17A920.

- [21] D.T. Cam Thanh, E. Brück, O. Tegus, J.C.P. Klaasse, T. J. Gortenmulder, K.H.J. Buschow, J. Appl. Phys. 99 (2006) 08Q107.
- [22] Yue Ming, Zhang Hong-Guo, Liu Dan-Min, Zhang Jiu-Xing, Chin. Phys. B 24 (2014) 017505.
- [23] Keiichi Koyama, Masanari Sakai, Takeshi Kanomata, Kazuo Watanabe, Jpn. J. Appl. Phys. 43 (2004) 8036.
- [24] K. Liu, S.C. Ma, L. Zhang, Y.L. Huang, Y.H. Hou, G.Q. Zhang, W.B. Fan, Y.L. Wang, Y. Wang, J. Cao, K.X. Guo, Z.C. Zhong, J. Alloys Compd. 690 (2017) 663.

ACCEPTED MANUSCRIPT

FIGURE CAPTIONS

Fig. 1. Temperature dependence of the magnetization measured at 5 mT for as-solidified $\text{Mn}_{1-x}\text{Cr}_x\text{CoGe}$ melt-spun ribbons with $x = 0.04$ and 0.11 . The corresponding room temperature X-ray powder diffraction patterns are shown in the top and bottom panels of the inset, respectively.

Fig. 2. Heating and cooling DSC (a) and $M(T)$ curves measured at 5 mT (b) in the temperature range of the first-order structural transformation for $\text{Mn}_{1-x}\text{Cr}_x\text{CoGe}$ melt-spun ribbons with $x = 0.04$. The vertical dashed lines indicate T_C^{hex} and RT, respectively. To facilitate the identification and correspondence between DSC and $M(T)$ curves, we set over the heating/cooling DSC pathways the same symbol and color used for the measured experimental points of the $M(T)$ curves.

Fig. 3. Heating and cooling DSC (a) and $M(T)$ curves measured at 5 mT (b) in the temperature range of the first-order structural transformation for $\text{Mn}_{1-x}\text{Cr}_x\text{CoGe}$ melt-spun ribbons with $x = 0.11$. The vertical dashed lines indicate T_C^{hex} and RT, respectively. To facilitate the identification and correspondence between DSC and $M(T)$ curves, we set over the heating/cooling DSC pathways the same symbol and color used for the measured experimental points of the $M(T)$ curves.

Fig. 4. Room temperature X-ray powder diffraction patterns for $\text{Mn}_{1-x}\text{Cr}_x\text{CoGe}$ melt-spun ribbons with $x = 0.04$ annealed at 923 K (a), 1123 K (b), and 1148 K [(c) and (d); 4 and 8 h, respectively]. The XRD reflections of the hexagonal Ni_2In -type and orthorhombic TiNiSi -type phases are denoted by H and O, respectively.

Fig. 5. Room temperature X-ray powder diffraction patterns for $\text{Mn}_{1-x}\text{Cr}_x\text{CoGe}$ melt-spun ribbons with $x = 0.11$ annealed at 923 K (a), 1123 K (b) and 1148 K [(c) and (d)]. The XRD reflections of the hexagonal Ni_2In -type and orthorhombic TiNiSi -type phases are denoted by H and O, respectively.

Fig. 6. DSC curves measured during the first cooling, first heating and second cooling for $\text{Mn}_{1-x}\text{Cr}_x\text{CoGe}$ melt-spun ribbons with $x = 0.11$ annealed at 923 K during 4 hours. The SEM micrographs, shown below, were taken at various temperatures during the first cooling of the sample from room temperature.

Fig. 7. Heating and cooling DSC and $M(T)$ curves measured at 5 mT (a) for $\text{Mn}_{1-x}\text{Cr}_x\text{CoGe}$ melt-spun ribbons with $x = 0.04$ annealed during 4 h at 1148 K and the corresponding room temperature (RT) X-ray powder diffraction patterns for water-quenched samples [(b); 300 K - A] and samples cooled to 193 K and warmed to RT [(c); 300 K - B]. The vertical dashed lines in (a) indicate T_C^{hex} and RT, respectively. The XRD reflections of the hexagonal Ni_2In -type and orthorhombic TiNiSi -type phases are denoted by H and O, respectively.

Fig. 8. Isothermal magnetization curves measured at selected temperatures through the orthorhombic to hexagonal transition for $\text{Mn}_{1-x}\text{Cr}_x\text{CoGe}$ ribbons thermally annealed at 1148 h during 8 hours: (a) and (b) curves measured on increasing the magnetic field up to 5 T for samples with $x = 0.04$ and 0.11, respectively. (c) and (d) curves measured on increasing the magnetic field up to 2 T (field-up) and removing the field to zero (field-down) for samples with $x = 0.04$ and 0.11, respectively.

Fig. 9. Temperature dependence of the magnetic isothermal entropy change for $\text{Mn}_{1-x}\text{Cr}_x\text{CoGe}$ ribbons with $x = 0.04$ (a) and 0.11 (b) annealed at various temperatures during 4 and 8 h for a magnetic field change of 2 and 5 T. Inset: Typical heating and cooling $M(T)$ curves measured at 5 T for the samples studied.

Table 1. Starting and finishing temperatures of the direct and reverse MT and thermal hysteresis ΔT_{hys} (estimated as $\Delta T_{\text{hys}} = A_f - M_S$) determined from the DSC curves for annealed $\text{Mn}_{1-x}\text{Cr}_x\text{CoGe}$ ($x = 0.04$ and 0.11) melt-spun ribbons. The $|\Delta S_M^{\text{peak}}|$ temperature as well as R_{exp} and χ^2 values of the Rietveld refinement for the thermally annealed samples are also listed.

Annealing parameters	T_C^{hex} (K)	T_C^{orth} (K)	M_S (K)	M_f (K)	A_S (K)	A_f (K)	ΔT_{hys} (K)	T for $ \Delta S_M^{\text{peak}} $ (K)	XRD fitting data	
									R_{exp}	χ^2
$\text{Mn}_{0.96}\text{Cr}_{0.04}\text{CoGe}$										
923 K - 4 h	225	-	374	318	370	404	30	313	22.9	2.2
1123 K - 4 h	225	-	285	255	298	315	30	306	14.0	2.1
1148 K - 4 h	225	-	295	269	301	324	29	310	22.5	2.0
1148 K - 8 h	225	-	274	249	281	299	25	291	28.4	1.7
<hr/>										
BULK 1123 K 120 h [10]	-	-	320*	301*	313*	330*	10*	319*	-	-
<hr/>										
$\text{Mn}_{0.89}\text{Cr}_{0.11}\text{CoGe}$										
923 K - 4 h	255	315	342	306	352	377	35	338	20.6	2.8
1123 K - 4 h	255	315	291	252	280	312	21	299	20.3	1.0
1148 K - 4 h	255	315	297	268	301	323	26	310	9.6	2.3
1148 K - 8 h	255	315	281	259	278	310	29	303	18.6	2.6
<hr/>										
BULK 1123 K 120 h [10]	-	-	270*	288*	301*	282*	12*	287*	-	-

*Values estimated from the $M(T)$ curves measured at 0.1 T reported [10,15].

Table 2. Maximum of magnetic field induced total entropy change, $|\Delta S_M^{\text{peak}}|$, useful working temperature range ($\delta T_{\text{FWHM}} = T_{\text{hot}} - T_{\text{cold}}$), and refrigerant capacity for a magnetic field change of 2 and 5 T for $\text{Mn}_{1-x}\text{Cr}_x\text{CoGe}$ melt-spun ribbons with $x = 0.04$ and 0.11 annealed at different temperatures.

Annealing parameters	$ \Delta S_M^{\text{peak}} $		δT_{FWHM}		RC-1		RC-2		RC-3	
	2T	5T	2T	5T	2T	5T	2T	5T	2T	5T
$\text{Mn}_{0.96}\text{Cr}_{0.04}\text{CoGe}$										
923 K 4 h	1.5	3.2	60	88	93	283	72	215	39	111
1123 K 4 h	3.6	8.8	24	25	86	224	68	178	52	115
1148 K 4 h	2.9	7.3	25	25	74	182	58	146	31	81
1148 K 8 h	4.2	10.6	22	22	93	235	73	185	-	-
BULK 1123 K										
120 h [10]	11.6	28.5	8*	8*	93	228	-	-	-	-
$\text{Mn}_{0.89}\text{Cr}_{0.11}\text{CoGe}$										
923 K 4 h	2.2	4.9	47	60	105	295	79	233	70	167
1123 K 4 h	3.9	9.7	21	21	82	203	49	122	-	-
1148 K 4 h	3.8	9.4	22	23	85	214	68	170	38	96
1148 K 8 h	5.6	13.7	18	18	106	267	85	214	-	-
BULK 1123 K										
120 h [10]	11	27.7	7*	7*	81*	203*	-	-	-	-

* Values estimated from the $\Delta S_M(T)$ curves reported in Ref. [10].

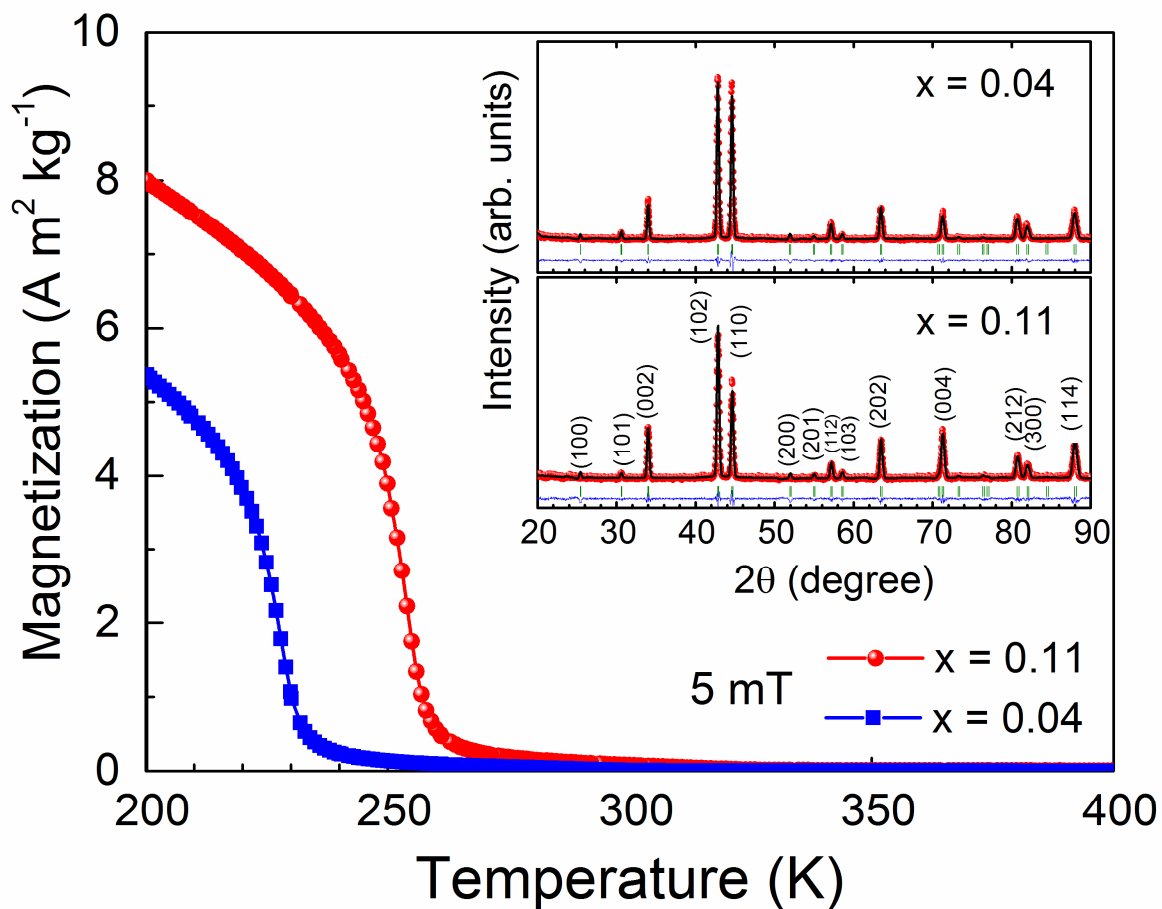


Fig. 1. Temperature dependence of the magnetization measured at 5 mT for as-solidified $\text{Mn}_{1-x}\text{Cr}_x\text{CoGe}$ melt-spun ribbons with $x = 0.04$ and 0.11 . The corresponding room temperature X-ray powder diffraction patterns are shown in the top and bottom panels of the inset, respectively.

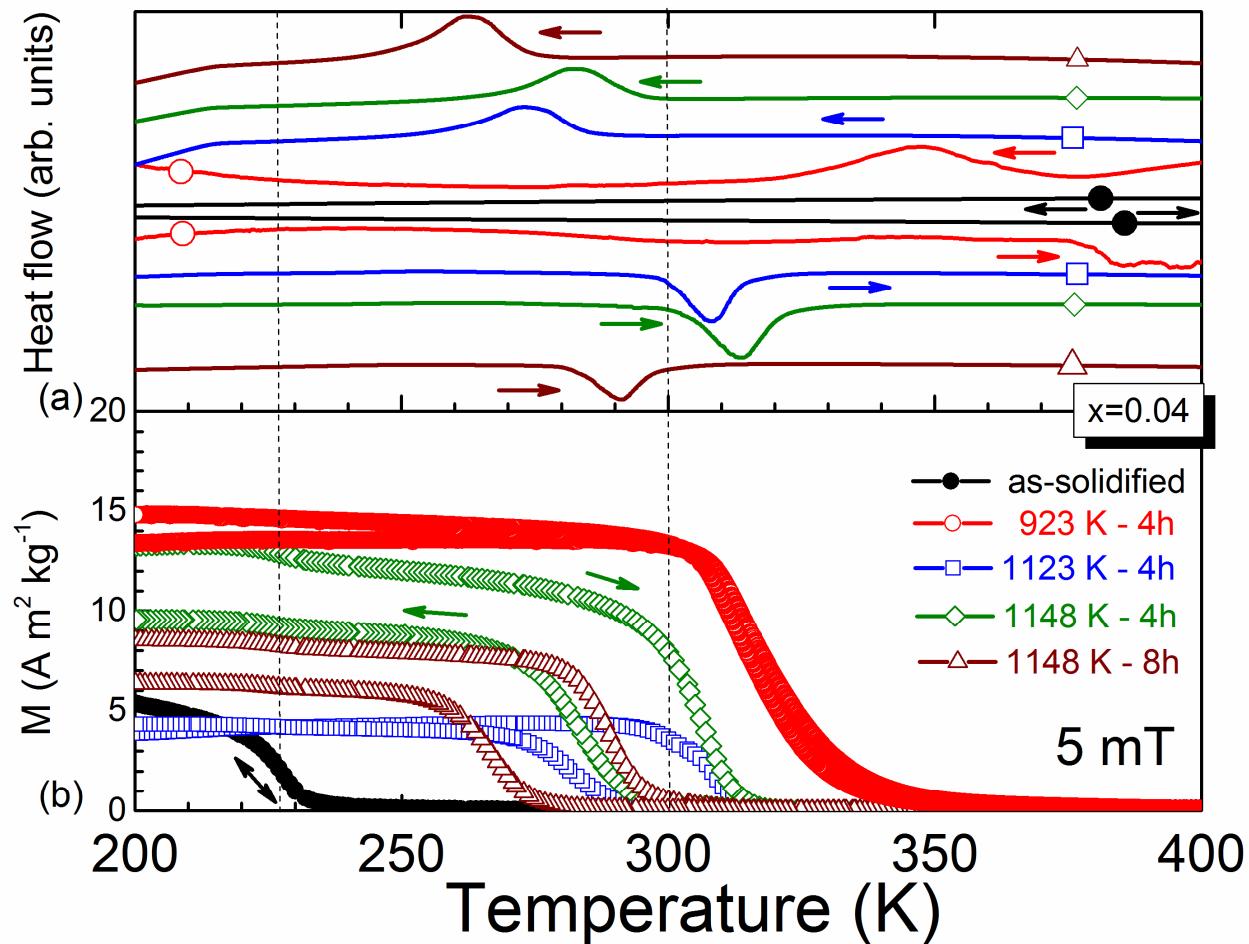


Fig. 2. Heating and cooling DSC (a) and $M(T)$ curves measured at 5 mT (b) in the temperature range of the first-order structural transformation for $\text{Mn}_{1-x}\text{Cr}_x\text{CoGe}$ melt-spun ribbons with $x = 0.04$. The vertical dashed lines indicate T_C^{hex} and RT, respectively. To facilitate the identification and correspondence between DSC and $M(T)$ curves, we set over the heating/cooling DSC pathways the same symbol and color used for the measured experimental points of the $M(T)$ curves.

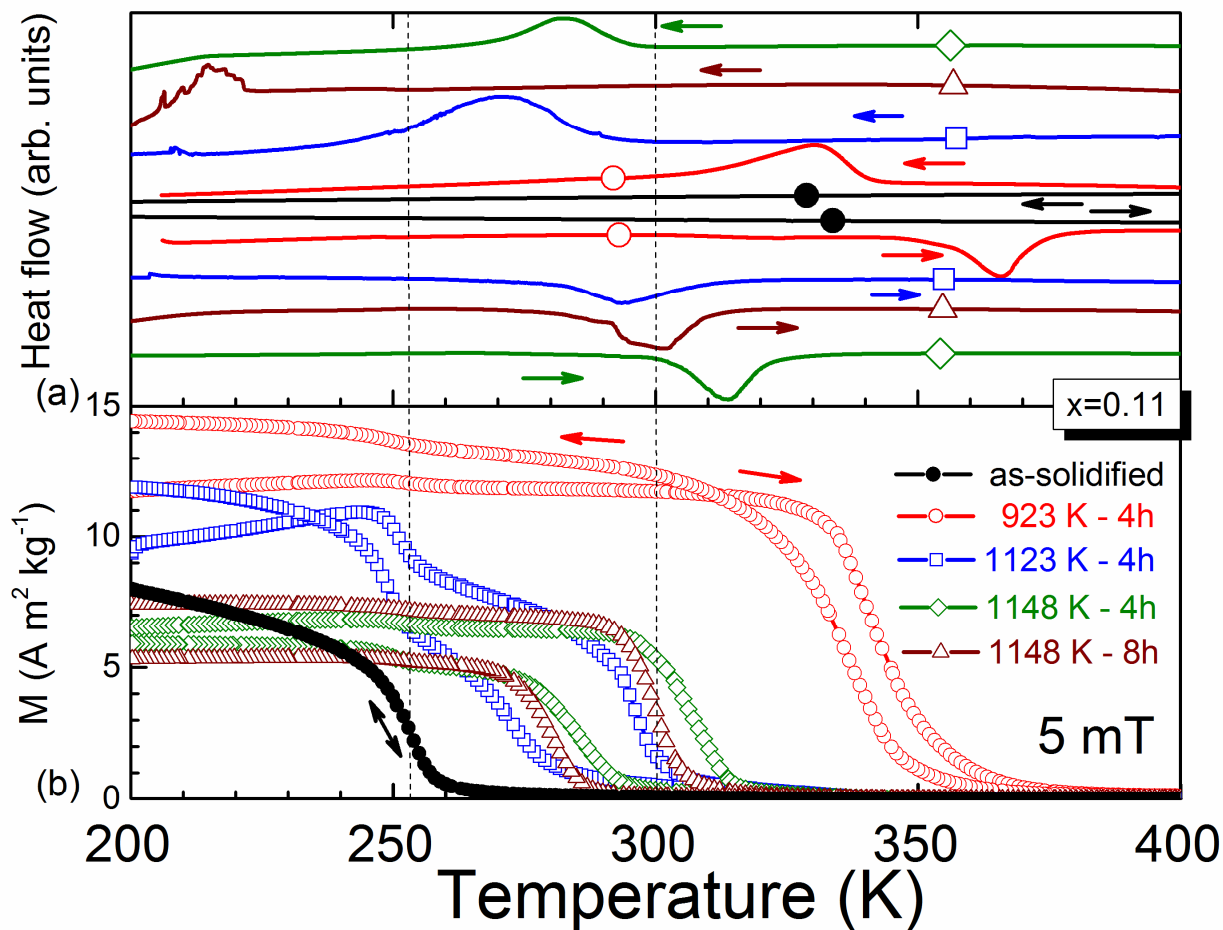


Fig. 3. Heating and cooling DSC (a) and $M(T)$ curves measured at 5 mT (b) in the temperature range of the first-order structural transformation for $\text{Mn}_{1-x}\text{Cr}_x\text{CoGe}$ melt-spun ribbons with $x = 0.11$. The vertical dashed lines indicate T_C^{hex} and RT, respectively. To facilitate the identification and correspondence between DSC and $M(T)$ curves, we set over the heating/cooling DSC pathways the same symbol and color used for the measured experimental points of the $M(T)$ curves.

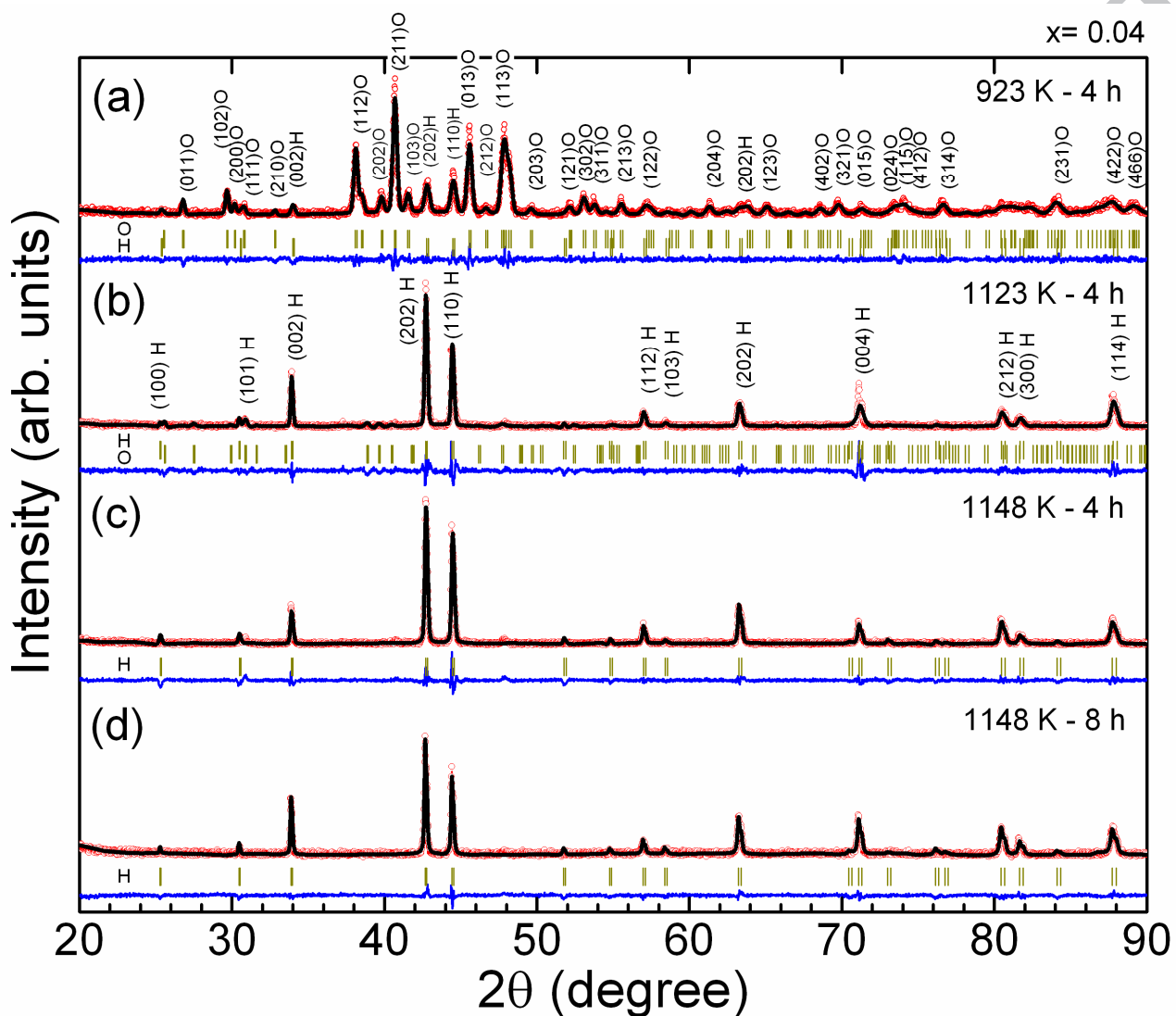


Fig. 4. Room temperature X-ray powder diffraction patterns for $\text{Mn}_{1-x}\text{Cr}_x\text{CoGe}$ melt-spun ribbons with $x = 0.04$ annealed at 923 K (a), 1123 K (b), and 1148 K [(c) and (d); 4 and 8 h, respectively]. The XRD reflections of the hexagonal Ni_2In -type and orthorhombic TiNiSi -type phases are denoted by H and O, respectively.

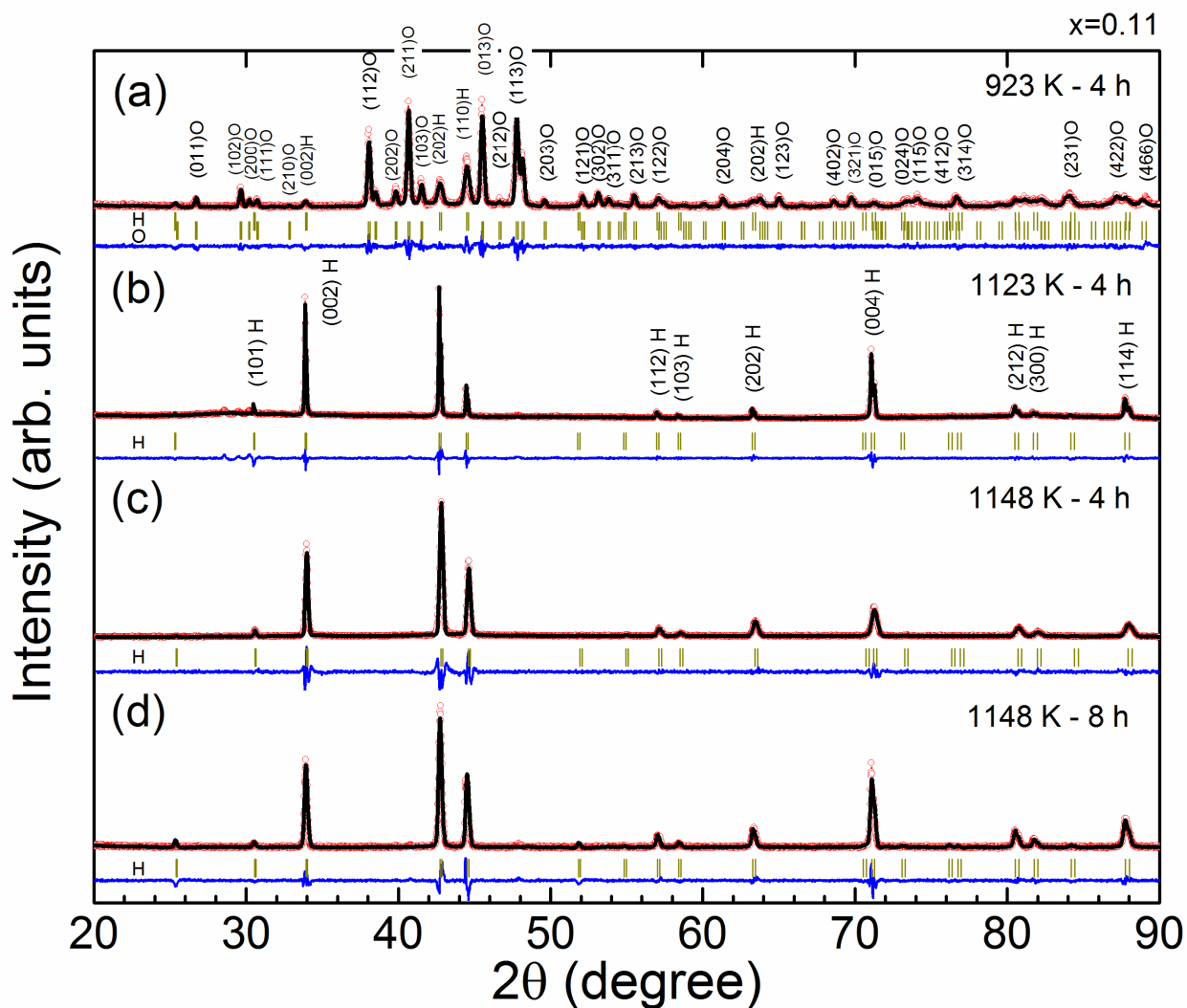


Fig. 5. Room temperature X-ray powder diffraction patterns for $\text{Mn}_{1-x}\text{Cr}_x\text{CoGe}$ melt-spun ribbons with $x = 0.11$ annealed at 923 K (a), 1123 K (b) and 1148 K [(c) and (d)]. The XRD reflections of the hexagonal Ni_2In -type and orthorhombic TiNiSi -type phases are denoted by H and O, respectively.

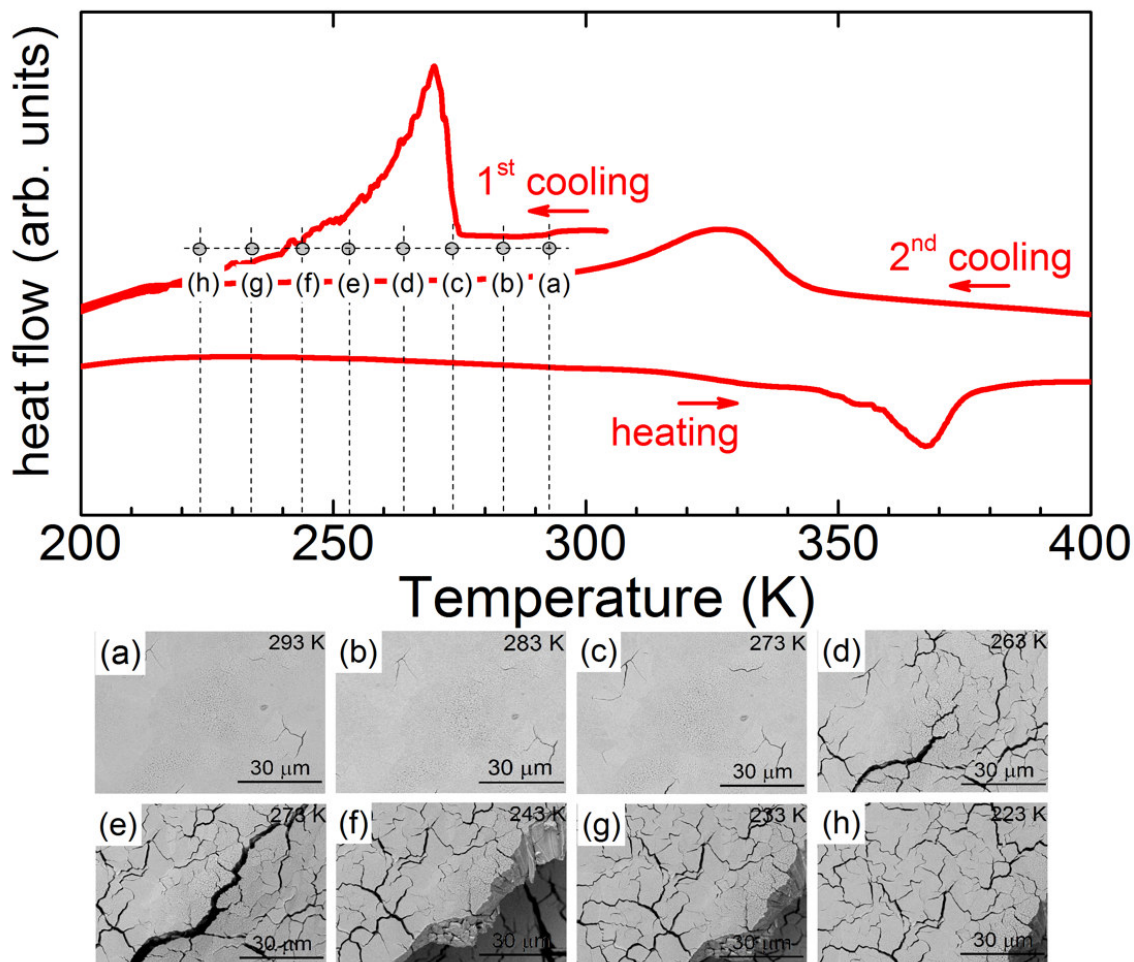


Fig. 6. DSC curves measured during the first cooling, first heating and second cooling for $\text{Mn}_{1-x}\text{Cr}_x\text{CoGe}$ melt-spun ribbons with $x = 0.11$ annealed at 923 K during 4 hours. The SEM micrographs, shown below, were taken at various temperatures during the first cooling of the sample from room temperature.

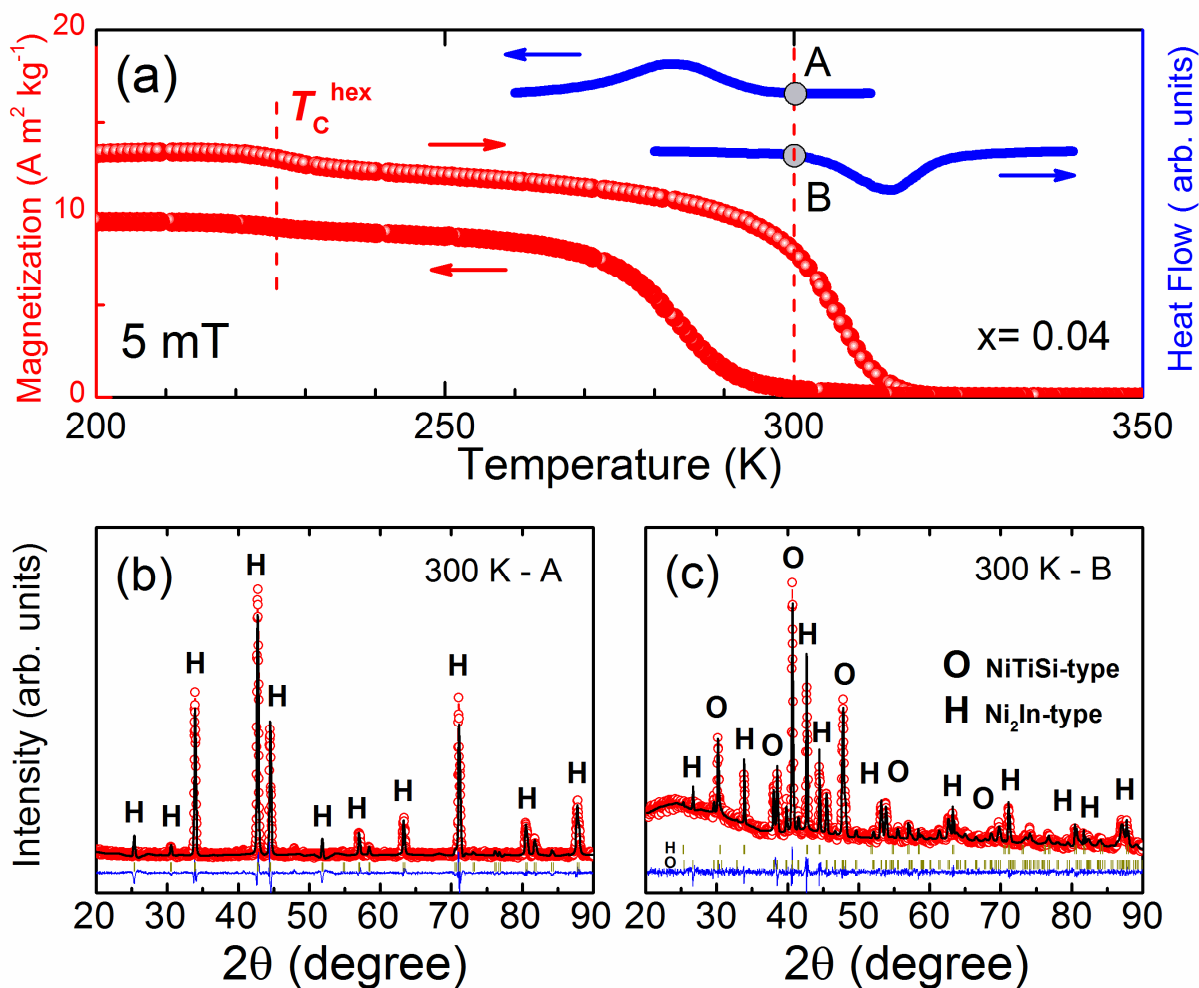


Fig. 7. Heating and cooling DSC and $M(T)$ curves measured at 5 mT (a) for $\text{Mn}_{1-x}\text{Cr}_x\text{CoGe}$ melt-spun ribbons with $x = 0.04$ annealed during 4 h at 1148 K and the corresponding room temperature (RT) X-ray powder diffraction patterns for water-quenched samples [(b); 300 K - A] and samples cooled to 193 K and warmed to RT [(c); 300 K - B]. The vertical dashed lines in (a) indicate T_C^{hex} and RT, respectively. The XRD reflections of the hexagonal Ni_2In -type and orthorhombic TiNiSi -type phases are denoted by H and O, respectively.

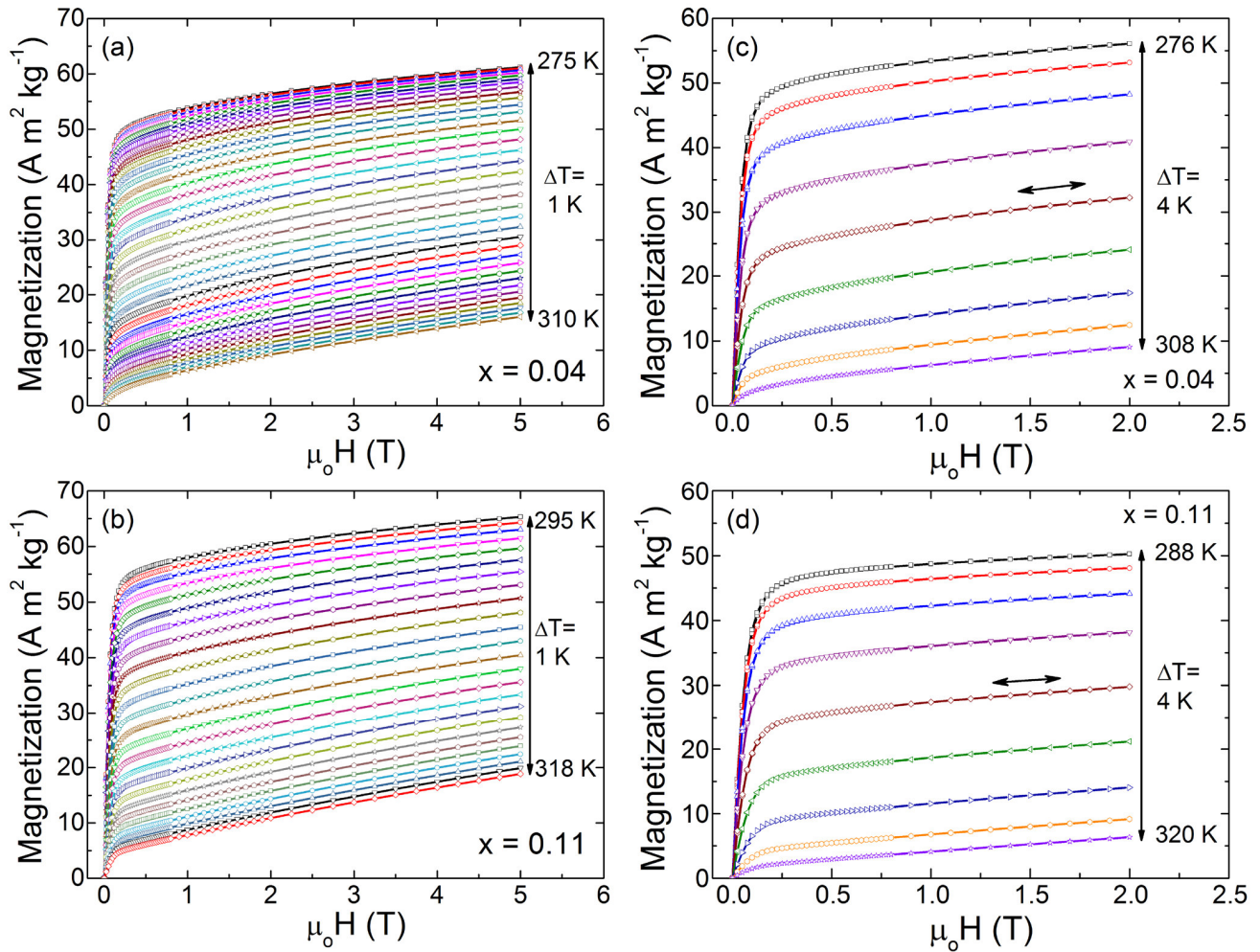


Fig. 8. Isothermal magnetization curves measured at selected temperatures through the orthorhombic to hexagonal transition for $\text{Mn}_{1-x}\text{Cr}_x\text{CoGe}$ ribbons thermally annealed at 1148 h during 8 hours: (a) and (b) curves measured on increasing the magnetic field up to 5 T for samples with $x = 0.04$ and 0.11, respectively. (c) and (d) curves measured on increasing the magnetic field up to 2 T (field-up) and removing the field to zero (field-down) for samples with $x = 0.04$ and 0.11, respectively.

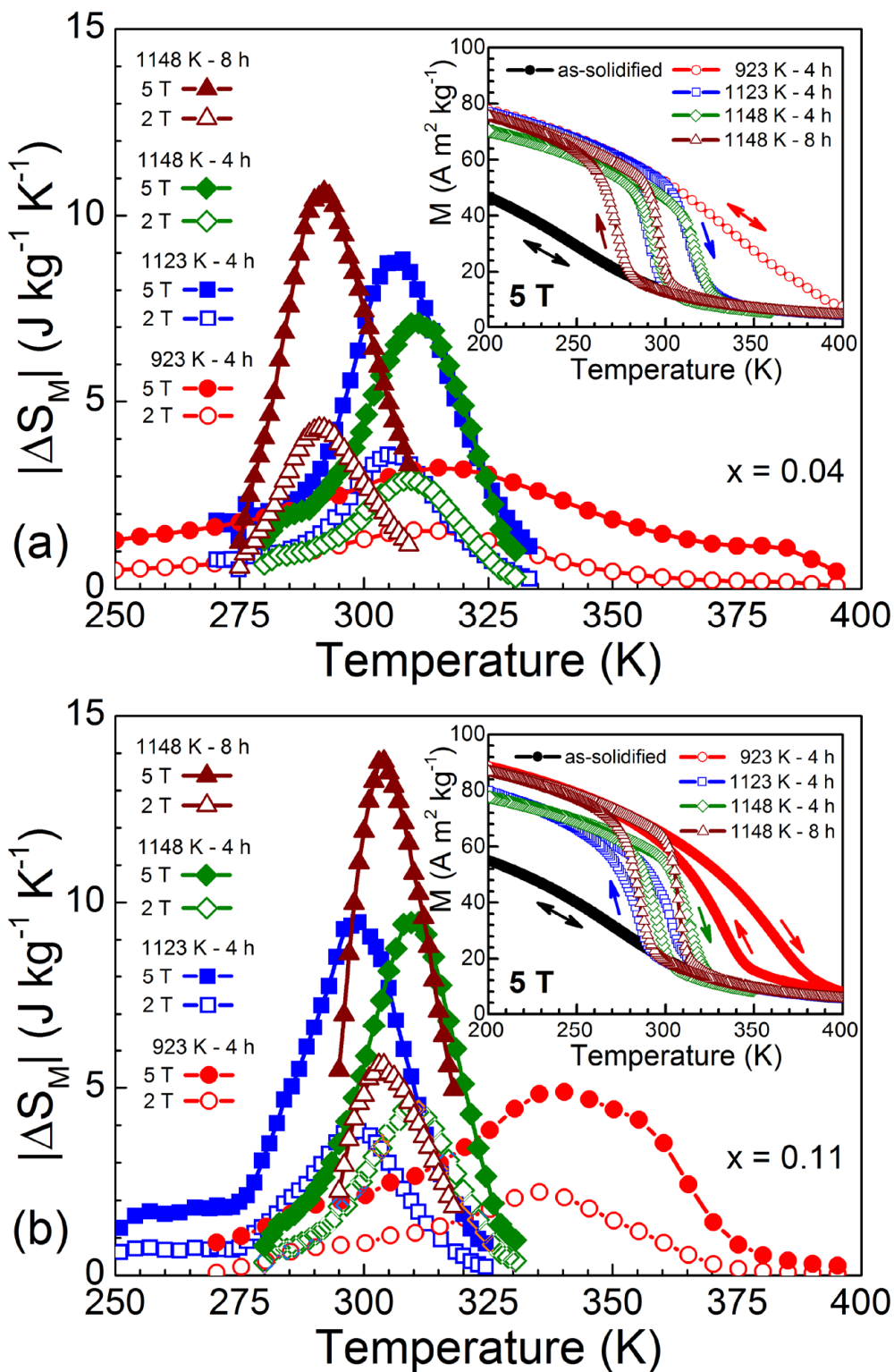


Fig. 9. Temperature dependence of the magnetic isothermal entropy change for $\text{Mn}_{1-x}\text{Cr}_x\text{CoGe}$ ribbons with $x = 0.04$ (a) and 0.11 (b) annealed at various temperatures during 4 and 8 h for a magnetic field change of 2 and 5 T. Inset: Typical heating and cooling $M(T)$ curves measured at 5 T for the samples studied.

Highlights

Mn_{1-x}Cr_xCoGe (x = 0.04 and 0.11) melt-spun ribbons were prepared and studied.

Varying temperature and time of annealing, the martensitic transformation and ferromagnetic transition of austenite were adjusted to be merged near room temperature.

Large magnetocaloric effect with much broader working temperature range and a higher cooling efficiency than bulk alloys of similar composition has been obtained.

ACCEPTED MANUSCRIPT